Research Article

Yi Zhang*, Qizhi Zhang, Muwaffaq Alqurashi, Ali H. AlAteah, and Ahmed A. Abdou Elabbasy

Leveraging waste-based additives and machine learning for sustainable mortar development in construction

https://doi.org/10.1515/rams-2025-0143
received June 18, 2025; accepted August 04, 2025

Abstract: This study presents a novel data-driven approach to improving the compressive strength (C-S) of environmentally friendly rubberized mortar that incorporates ingredients that are in line with current sustainability objectives in construction: glass powder, marble powder, and silica fume. Our predictive models were built using state-of-the-art machine learning (ML) approaches, specifically gene expression programming (GEP) and multi-expression programming (MEP), employing a thorough experimental dataset. Thorough evaluations of the models were conducted using important statistical metrics, such as the R^2 coefficient, root mean square error, and mean absolute error. The use of individual conditional expectation plots and partial dependence plots allowed for both individual and average variable effect studies, which were conducted to improve interpretability. Despite the good performance of the GEP model (R^2 = 0.91), the MEP model proved to be more effective in capturing complicated, nonlinear connections with its superior accuracy and generalization (R^2 = 0.95). ML has the ability to greatly improve sustainable construction practices by reducing the need for experiments, speeding up the process of mix optimization, and encouraging the creation of cementitious composites that are less harmful to the environment. The findings contribute to the construction sector by integrating digital innovation with material sustainability.

Keywords: rubberized mortar, sustainable construction materials, gene and multi-expression programming

1 Introduction

The construction sector accounts for nearly 33% of the global CO_2 emissions, with concrete being a major contributor [1,2]. Reducing the carbon footprint of building materials is vital for promoting sustainable construction, especially in developing countries [3]. National and international bodies are working to minimize the use of primary resources and boost recycling as part of efforts to reduce emissions and support a circular economy [4–6]. One such initiative is the UN's industrial symbiosis systems, which encourage the reuse of industrial byproducts across sectors [7]. The United Nations International System for Sustainable Solid Waste also promotes recycling of commonly discarded construction materials like rubber (Rb), plastic, glass powder (Gp), silica fume (S-F), and marble powder (Mp) to curb landfill overflow and resource depletion [8]. Among these, rubber from used tires has gained attention due to the environmental issues associated with burning or dumping them [9,10]. Replacing natural aggregates or cement with recycled Rb has shown promise in enhancing sustainability. Studies have evaluated the effects of adding Rb to concrete and mortar on properties such as toughness, compressive and tensile strength, energy absorption, and cracking behavior [7,11–15]. Although rubberized mortar has lower strength than conventional alternatives, its benefits make it suitable for non-load-bearing elements like precast blocks and partition walls [9,16–18].

Gp, S-F, Mp, and other supplemental cementitious materials (SCMs) have recently been the subject of extensive research as potential cement alternatives. Mp is readily available in many countries and can serve as a viable substitute for cement in both mortar and concrete mixtures [19]. Due to its durability, marble is frequently

* **Corresponding author: Yi Zhang**, School of Architecture and Engineering, Huanghuai University, ZhuMaDian, 463000, China, e-mail: jingminzhang1699@163.com
Qizhi Zhang: School of Architecture and Engineering, Huanghuai University, ZhuMaDian, 463000, China
Muwaffaq Alqurashi: Department of Civil Engineering, College of Engineering, Taif University, P.O. Box 11099, Taif, 21944, Saudi Arabia
Ali H. AlAteah: Department of Civil Engineering, College of Engineering, University of Hafr Al Batin, Hafr Al Batin, 39524, Saudi Arabia
Ahmed A. Abdou Elabbasy: Civil and Architectural Engineering Department, College of Engineering and Computer Sciences, Jazan University, P.O. Box 706, Jazan, 45142, Saudi Arabia

utilized for a range of non-structural items, including architectural embellishment, cladding, sculpture, and flooring. In the course of carving and cutting marble for various purposes, a great deal of debris, mostly dust, is produced. Degradation of natural habitats and ecosystems is accelerated by these materials. The amount of cement or aggregate that Mp can replace has been as high as 60%. The ferrosilicon industry produces S-F, a highly pozzolanic by-product, which can increase the strength and longevity of concrete [20]. Adding small amounts of S-F to the concrete mix instead of cement can result in high-performance concrete with remarkable mechanical properties, according to studies by Zhao and Zhang [21]. Murali *et al.* [22] studied how S-F and Gp-enhanced ultra-high-performance geopolymer concrete handled impacts. Cementitious mixes that contain S-F as an SCM undergo a chemical composition with calcium hydroxide as a result of cement hydration. This chemical composition ultimately results in the production of an additional gel made of calcium silicate hydrate [23]. It is possible to improve the material's strength characteristics and loading performance by adding S-F to a cementitious mixture. The remarkable mechanical and physical properties of SF have prompted extensive study of the material. Results demonstrated that, particularly at higher strain rates, cementitious composites' mechanical characteristics are significantly improved. According to earlier research [23], the most effective SCM is 10% S-F. This mix exhibits a C-S of around 32.5 MPa and a fracture tensile strength of approximately 3.45 MPa. After this stage, adding additional S-F weakens the mixture.

The use of Gp, Mp, and Rb in conventional concrete and mortar has been the subject of numerous scholarly investigations. The effects of S-F on cementitious composites have also been the subject of extensive research, and a recent review article synthesized this literature [24]. However, no one has ever looked at how all of these things work together to affect the strength of cement mortar, particularly when it comes to optimizing them using cutting-edge AI/ML methods [25]. The emergence of soft computing has significantly improved the ability to simulate and predict the technical behavior of various materials with greater precision. Machine learning (ML) models, in particular, rely on input datasets to generate accurate forecasts. However, construction materials present a unique challenge due to their complex nature and inherent variability, making precise evaluation difficult. Among the many applications of ML in the construction sector, one of the most prominent is the prediction and assessment of the engineering properties of materials. Researchers have applied these techniques to study both traditional and modern types of concrete, achieving valuable insights into their performance characteristics. Among these varieties of concrete are those that use phase change materials, lightweight concrete, self-compacting concrete, fiber-reinforced concrete, and recycled aggregate concrete [26–30]. Multiple studies have demonstrated that when precisely evaluating certain engineering features, robust ML models outperform more conventional physical and empirical approaches. In order to obtain reliable predictions about the properties of concrete, specific computational obstacles must be overcome. Problems arise because of the complex processes involved in cement hydration and microstructure creation, and the non-linear correlation among the temperature, time, and cement paste activity [31–33]. For accurate attribute prediction, ML models must be trained with a combination of proportion and curing condition data. Predictions made with ML models are accurate, reproducible, and generalizable, and they also require little processing power and are easy to use [34].

In order to forecast the extent of concrete C-S using preexisting statistics, this research employs two ML algorithms: gene expression programming (GEP) and multi-expression programming (MEP). Several statistical measures, such as the R^2 coefficient, the error distribution, and other quantitative assessments, are used to evaluate the two models' predictive accuracy. The main objective is to calculate the predictive power of ML for material properties, namely C-S, by analyzing the experimental data for six critical input factors. Sophisticated visualization techniques were employed, like partial dependence plots (PDPs) and individual conditional expectation (ICE) studies, to understand the model's behavior and determine how each variable affects it. Better material performance prediction and informed decision-making in concrete production can be achieved by using the insights obtained from these models, which can improve existing databases on supplementary cementitious materials (SCMs) and direct the creation of optimum concrete mix designs.

2 ML framework

2.1 Overview of data and analytical strategy

The development of robust data-driven predictive models critically depends on the availability of a reliable and comprehensive dataset [35]. In this study, a curated dataset comprising 408 experimental records on rubberized mortar has been compiled from a reputable, peer-reviewed international publication [36]. The dataset includes six key input variables identified as significant predictors of C-S: cement (CM), sand (Sd), rubber (Rb), silica fume (S-F), marble powder (Mp), and glass powder (Gp). These input parameters, expressed in kilograms per cubic

meter ($kg \cdot m^{-3}$), were systematically selected based on their relevance and frequency of use in the literature. The target output variable is the C-S, reported in megapascals (MPa). These input features and the output variable are illustrated schematically in Figure 1. This dataset serves as the foundational input for training and evaluating the predictive algorithms employed in this study.

2.1.1 Data distribution and splitting

It has been proposed multiple times that the dataset for model development can be split into two or even three parts; one part of the dataset should be used for training the algorithms, and the other part should be utilized for testing their accuracy [37]. The collected dataset was divided into two segments: a training set comprising 286 data points (70%) and a testing set consisting of the remaining 122 data points (30%). For GEP, the dataset was automatically split into 70% training and 30% testing according to the software's default settings; for MEP, however, the data were manually separated into the same 70–30 ratio before the model was built. To ensure generalizability and avoid overfitting, ML models were first trained on the training set before being evaluated on the previously unseen testing data. An equally important aspect when developing data-driven models is the distribution of the dataset itself, as it plays a vital role in the accuracy and reliability of the model's predictive performance. An ML model's efficacy is proportional to the dispersion of the training data [38]. Marginal histograms in Figure 2(a)–(f) are visualization tools in ML that provide simultaneous insight into both the univariate distribution of individual variables and their bivariate relationships. Positioned above and to the right of a central scatter plot, these histograms help identify skewness, modality, and outliers in each variable, offering critical context for feature engineering and model selection. For instance, in the plot comparing CM (*x*-axis) and C-S (*y*-axis), the top histogram reveals that CM values predominantly cluster around 60–70, with a leftward tail indicating fewer low-value cases. The right histogram shows that C-S is concentrated between 40 and 50, with a slight right skew suggesting occasional higher values. The central scatter plot indicates a moderate positive correlation between CM and C-S, as higher CM values tend to correspond with higher C-S values, though with notable variability. This positive trend is reinforced by the lack of data points in the upper-left region, implying that high C-S values rarely occur with low CM. Such patterns suggest potential multicollinearity, which may influence model performance depending on the algorithm used. Overall, marginal histograms provide a compact yet rich summary of feature behavior, guiding preprocessing decisions such as normalization, transformation, and feature selection in a data-driven modeling workflow.

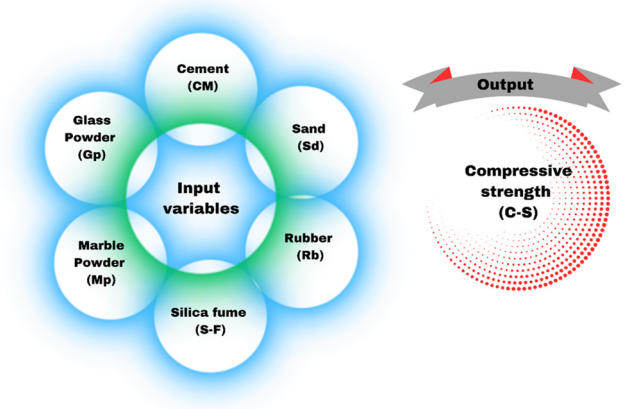

Figure 1: Overview of the input features and target output.

2.1.2 Variable correlation assessment

Checking the interdependence of the selected variables is a good first step before building the model. This is because input variables that are significantly related to one another might lead to multicollinearity, a problem that may emerge while developing algorithms [39]. Statistical analysis tools like correlation matrices allow researchers to verify the interdependence of study variables. The coefficient of correlation (R) measures the regression between several variables, making it useful for checking the interdependence of explanatory factors. One can see how dependent one variable is on the other by observing the R-value between them. When this R-value is positive, it means that the two variables are positively correlated; when it is negative, it indicates that the opposite is true. In most cases, a high level of correlation between the two variables is indicated by an R value higher than 0.8 [40]. In most instances, the correlation values between different variables are less than 0.8, as can be seen from the correlation matrix that was generated for the data utilized in this study (Figure 3). This means that developing the model will not put one at risk of multicollinearity.

2.2 ML modeling

The final output of a procedure requiring six inputs, the C-S of rubberized mortar, was the subject of laboratory analysis. The GEP and MEP models are examples of modern ML techniques that could permit the correct prediction of the C-S of

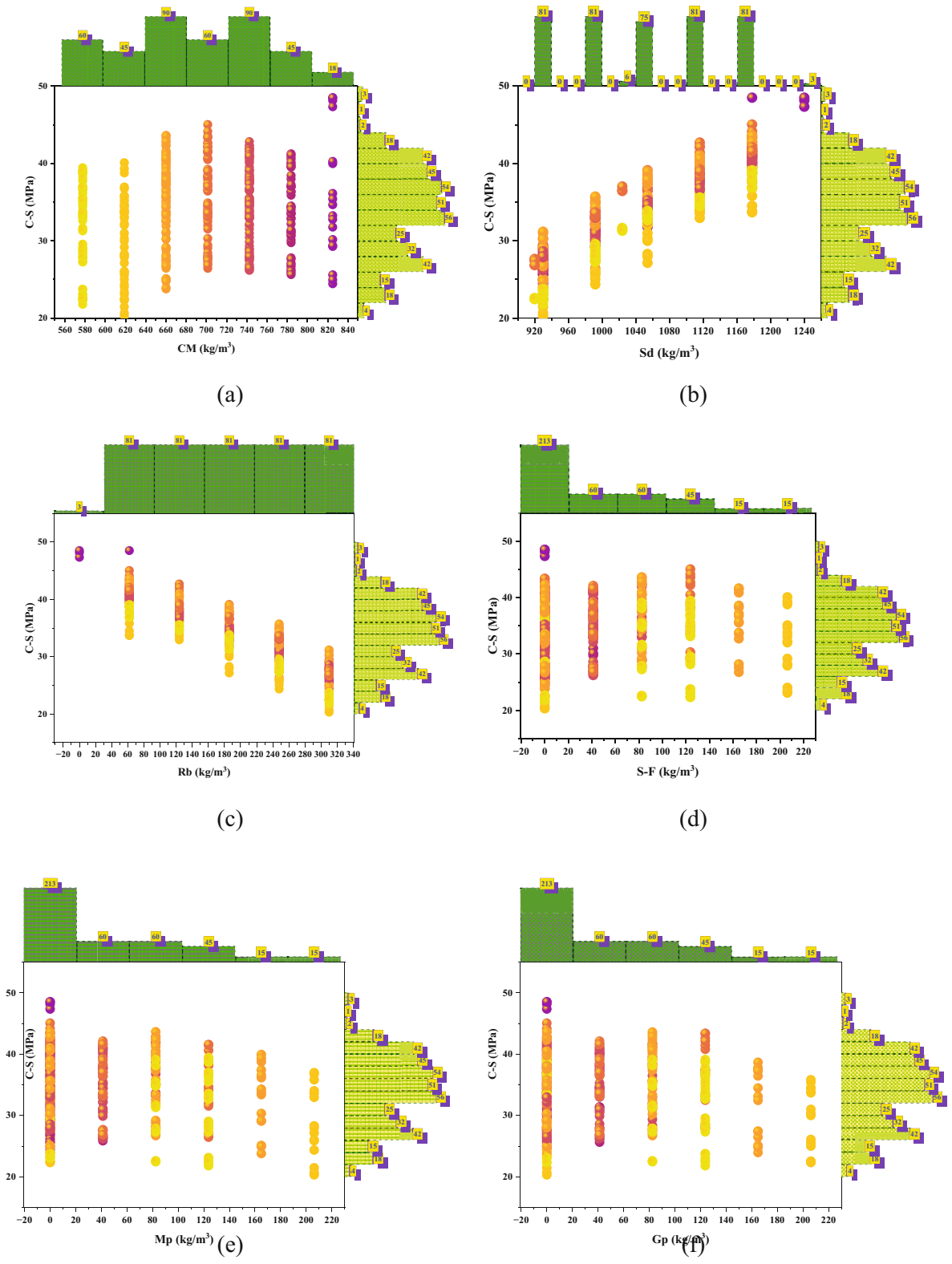

Figure 2: Input and output data distributions *via* marginal histograms: (a) CM, (b) Sd, (c) Rb, (d) S-F, (e) Mp, and (f) Gp.

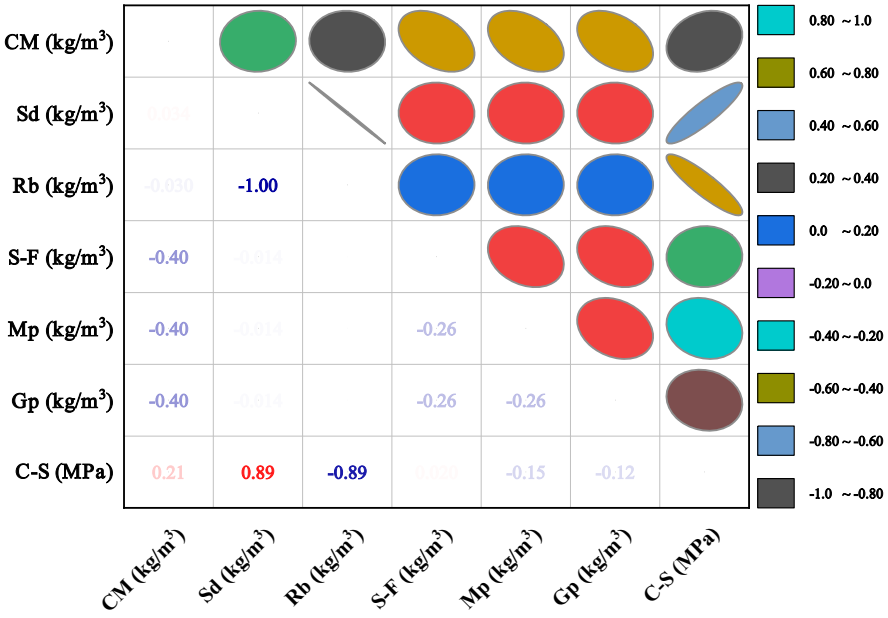

Figure 3: Correlation matrix of variables.

rubberized mortar. ML algorithms are typically evaluated by observing the input data. Seventy percent of the data from this investigation went toward training the models, while thirty percent was utilized for testing. The level of agreement between the predicted and actual results is strongly correlated with the R^2 value; a low value suggests a substantial discrepancy [41], acknowledging the practicality of the models. Additional approaches were utilized to check the model's correctness, like statistical tests and error evaluations. Table 1 presents an overview of the key hyperparameters used in configuring the GEP and MEP models. These parameters were selected through a trial-and-error approach to achieve the best model fit for the given dataset. Figure 4 illustrates a simplified diagram of the event modeling process.

2.2.1 GEP model

Computer programs able to solve complicated issues can be evolved using GEP, an evolutionary technique initially presented by Ferreira [42,43]. Important components of the GEP technique are as follows:

1) **Preliminary population generation:** The process originates with the creation of a random populace of chromosomes. Each chromosome encodes a computer program in the form of symbolic sequences, representing mathematical models or algorithms.
2) **Fitness assessment:** A fitness score, which indicates how well a chromosome solves the challenge at hand, is computed for each one. Here, fitness is defined as a chromosome's ability to predict the C-S of rubberized mortar.
3) **Evolutionary selection phase:** Chromosomes that are more suited for reproduction are chosen for reproduction if they provide fewer prediction mistakes. These individuals embody the most qualified applicants from the present crop.
4) **Genetic operations:** Mutations, which change gene sequences, and crossovers, which involve the exchange of segments between chromosomes, are examples of

Table 1: MEP/GEP method parameters

Groups	Descriptions	Settings
GEP/MEP sampling	Training records	286
	Validation/test records	122
GEP parameters	Error measure	MSE
	Number of sub-populations	100
	Sub-population size	250
	Code length	50
	Cross-over probability	0.9
	Number of generations	250
	Mutation probability	0.1
	Functions	+, −, ÷, ×, √, ^, e^x
MEP parameters	Number of chromosomes	75
	Head size	10
	Number of genes	6
	Linking function	Addition
	Functions	+, −, ÷, ×, √, ^, e^x

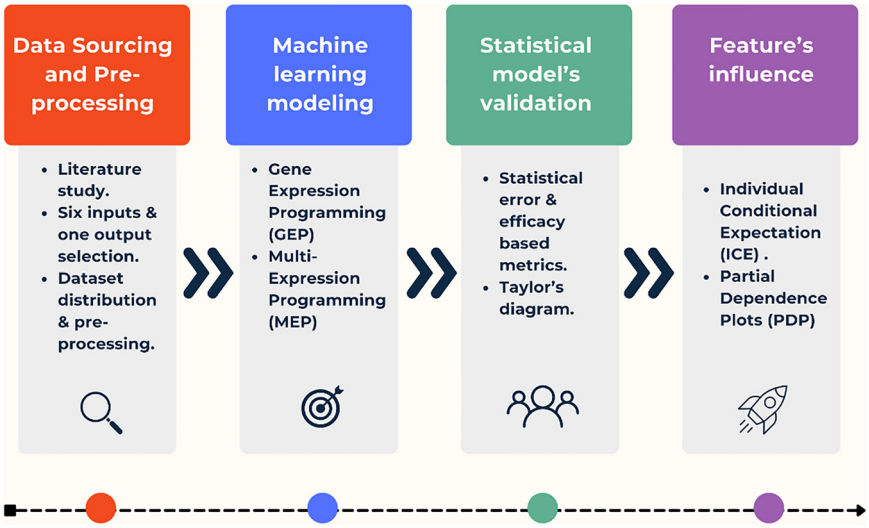

Figure 4: Step-by-step workflow of the adopted methodology.

genetic operators that modify some chromosomes. These processes produce new generations, which may have enhanced capabilities.

5) **Progression through generations:** Over the course of many generations, the population is able to evolve and become better at addressing problems because of the iterative cycle of fitness assessment, selection, and genetic processes.
6) **Final model output:** Mathematical expressions optimized from the training data are produced by GEP after several iterations. Predicting the intended material qualities with precision is made possible by these formulas. Figure 5 shows a schematic of the GEP procedure.

2.2.2 MEP model

A complex evolutionary algorithm, MEP, expands upon genetic programming principles, including those outlined in GEP [45]. Phases that make up the MEP process are as follows:

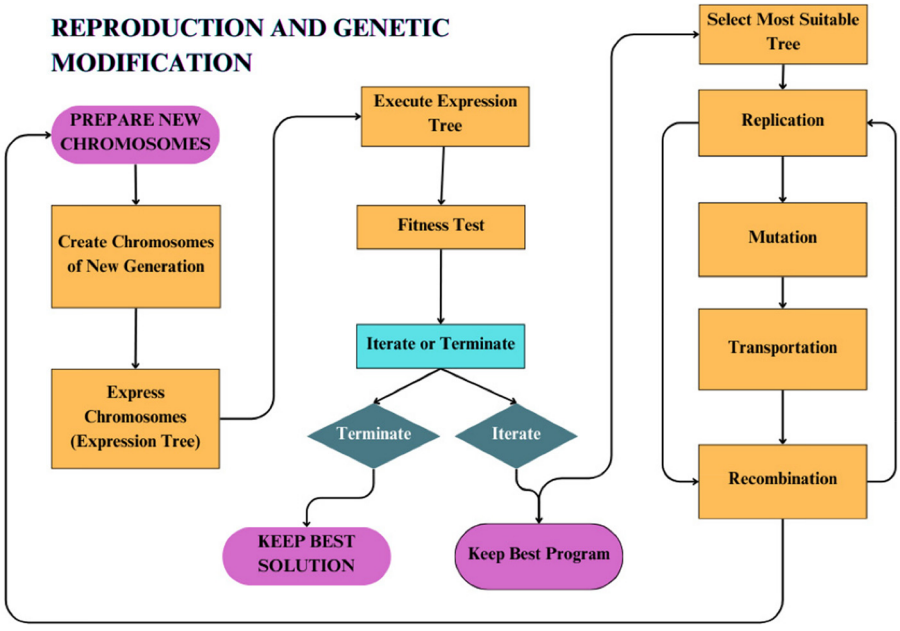

Figure 5: Process flow of the GEP-based model development [44].

1) **Preliminary population generation:** As with GEP, MEP originates by generating a random population of chromosomes. However, a distinctive feature of MEP is that each chromosome encodes several potential mathematical expressions simultaneously.
2) **Fitness evaluation:** Every expression within a chromosome is individually assessed for its fitness, which reflects how accurately it addresses the prediction task.
3) **Selection of best performers:** The most effective expressions – those with the highest fitness – are selected as parents to form the next generation, ensuring the continued propagation of strong solutions.
4) **Genetic modification:** Selected expressions undergo genetic operations such as mutation and crossover. These modifications result in new offspring that may offer enhanced predictive capabilities.
5) **Evolution over generations:** Over the course of several generations, the population's performance is fine-tuned through this iterative cycle of fitness evaluation, selection, and genetic alteration.
6) **Evolved solutions:** Optimal expression generation is the last step in MEP, which leads to precise forecasts of target qualities like rubberized mortar's C-S. Figure 6 shows the MEP workflow graphically.

2.3 Model validation

The models developed through GEP and MEP were assessed statistically using a designated test dataset. To determine the performance of each model, seven distinct statistical metrics were calculated [46–50], such as the root mean square error (RMSE), mean absolute error (MAE), mean absolute percentage error (MAPE), Pearson's correlation coefficient (R), Nash–Sutcliffe efficiency (NSE), performance index (PI), and objective function (OF). The mathematical formulations for these metrics are presented in Eqs. (1)–(7):

$$R = \frac{\sum_{i=1}^{n}(a_i - \bar{a}_i)(p_i - \bar{p}_i)}{\sqrt{\sum_{i=1}^{n}(a_i - \bar{a}_i)^2 \sum_{i=1}^{n}(p_i - \bar{p}_i)^2}}, \tag{1}$$

$$\text{MAE} = \frac{1}{n}\sum_{i=1}^{n}|p_i - a_i|, \tag{2}$$

$$\text{RMSE} = \sqrt{\sum \frac{(P_i - a_i)^2}{n}}, \tag{3}$$

$$\text{MAPE} = \frac{100\%}{n}\sum_{i=1}^{n}\frac{|P_i - a_i|}{a_i}, \tag{4}$$

$$\text{PI} = \frac{\frac{1}{|\bar{p}|}\sqrt{\frac{\sum_{i=1}^{n}(a_i - p_i)^2}{n}}}{R}, \tag{5}$$

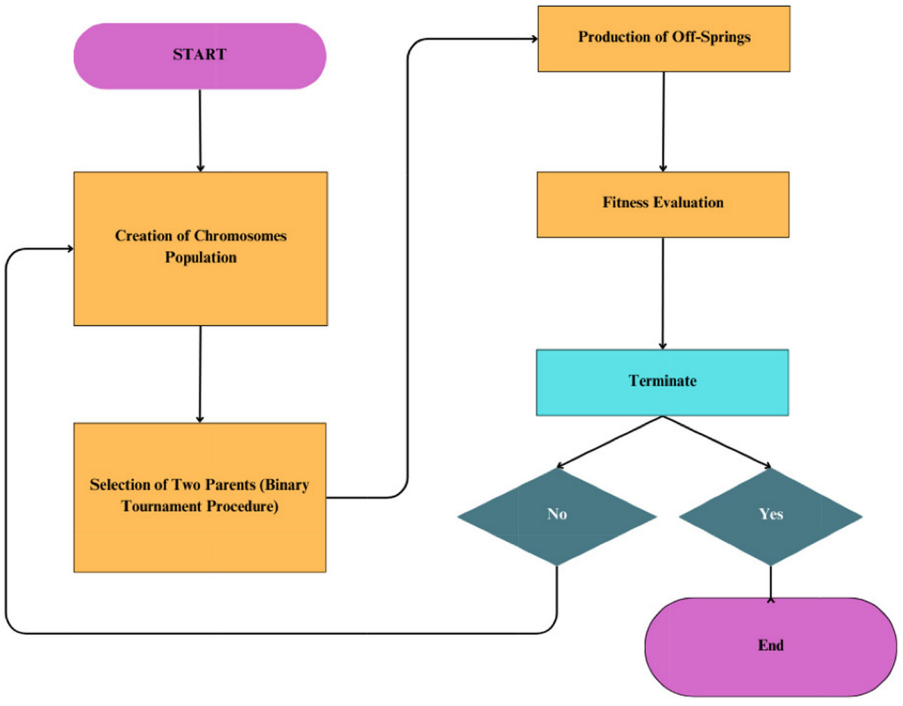

Figure 6: Flowchart of the MEP method [44].

$$\text{NSE} = 1 - \frac{\sum_{i=1}^{n}(a_i - p_i)^2}{\sum_{i=1}^{n}(a_i - \bar{p}_i)^2}, \tag{6}$$

$$\text{OF} = \left(\frac{n_{\text{train}} - n_{\text{test}}}{n}\right)\text{PI}_{\text{train}} + 2\left(\frac{n_{\text{test}}}{n}\right)\text{PI}_{\text{test}}, \tag{7}$$

where a_i are the observed values, $\bar{p}_i$ are the estimated values, n is the total data points, R, short for the correlation coefficient, is a commonly used metric to assess the predictive capability of a model by quantifying the association between test values (a_i) and estimated values (p_i). A higher R value indicates a stronger correlation between the predicted outputs and observed data, signifying better model performance [51]. The correlation coefficient (R) is unaffected by operations such as multiplication or division, making it a stable indicator of linear relationships. However, the coefficient of determination (R^2) was also computed by comparing predicted values to actual outcomes. This is because R^2 provides a more accurate measure of how well the model captures the variance in the data. An R^2 value close to 1 signifies a highly effective and reliable model [52,53]. Likewise, both MAE and RMSE showed strong performance, particularly when evaluated under conditions involving larger errors. Lower values of MAE and RMSE indicate fewer substantial deviations between predicted and actual values, with values nearing zero reflecting improved model accuracy [54,55]. Upon closer examination, it was observed that MAE performs particularly well with datasets that exhibit continuity and smooth variation, making it a reliable metric under such conditions [56]. The model generally demonstrates better performance when the magnitude and frequency of prior prediction errors are low.

In addition, the PI from Gandomi and Roke [57] was proposed, which can take values between zero and infinity. If the PI were to be smaller, it would mean that the model was more efficient. If the PI of a model is 0.2 or below, the author claims that it is satisfactory. To be considered adequate, a model's PI value must be less than 0.3. More often than not, ML models experience overfitting when they do exceptionally well on training data but fail miserably when presented with novel data. The study's solution to this problem is shown in Eq. (5), which makes use of the OF. To avoid overfitting, OF helps strike a compromise between minimizing errors in the training data and guaranteeing that the model can be applied to new data.

The Taylor diagram is not only used for statistical validation but also for visually evaluating the accuracy of models' predictions. By showing important performance measures like correlation, standard deviation, and RMSE all at once, it shows how well various models match the observed data that is used as a reference point. To find the most accurate and trustworthy models, this integrated visualization allows the comparison of precision and dependability in a straightforward and thorough way [58,59]. The Taylor diagram is a graphical tool used to evaluate model performance by incorporating three statistical measures: standard deviation represented by radial lines, correlation coefficient shown along the horizontal and vertical axes, and RMSE depicted as concentric circles centered on the reference point, which corresponds to the observed data. This diagram allows for a comprehensive comparison of different models. A model positioned closest to the reference point demonstrates the highest prediction accuracy, as it reflects a strong correlation, minimal deviation from the observed values, and a low RMSE [58].

3 Comparative analysis and results

3.1 C-S GEP model

The expression trees (ETs) in Figure 7(a)–(f) generated through the GEP model for predicting C-S represent a structured and interpretable formulation of how input variables influence the output. These ETs were constructed using a defined set of mathematical functions, including addition (+), subtraction (−), multiplication (×), division (÷), square root (√), exponentiation (^), and exponential (e^x), allowing the model to capture complex non-linear interactions among six input parameters: CM, Sd, Rb, S-F, Gp, and Mp. Through evolutionary optimization, the model selected and combined these variables to produce an accurate and generalized mathematical expression. The final equation derived from these ETs, presented as Eq. (8), incorporates nested and compound operations, effectively modeling the interdependencies between materials. In addition to providing precise predictions, this equation sheds light on material behavior, which is crucial for making educated choices on sustainable material design and optimizing mix formulations.

Figure 8(a) presents a scatter plot comparing the predicted C-S values against experimental results, showing an excellent linear alignment around the ideal $y = x$ line. This strong correlation is quantified by an R^2 (coefficient of determination) value of 0.91, indicating that 91% of the variability in the experimental data is captured by the GEP model. The near-unity slope (0.93) and a modest intercept (4.37) further affirm the model's reliability and minimal bias, reflecting its high prediction accuracy. As shown in Figure 8(b), the left sub-figure combines line and symbol plots for both experimental and predicted compressive strengths, with a third

trace illustrating the absolute error. The visual overlap between the predicted and experimental trends suggests strong agreement throughout the dataset. Moreover, the right-side plot in Figure 8(b) shows the absolute error across samples, which, although varying, generally remains within an acceptable range, signifying that the GEP model is not only accurate on average but also consistent across diverse mix compositions. The maximum absolute error was 4.535 MPa, while the minimum error was a negligible 0.007 MPa, with an overall average of 1.435 MPa. Out of all data points, 48 samples exhibited errors less than 1 MPa, 50 samples had errors between 1 and 2 MPa, and only 38 samples exceeded the 2 MPa error threshold. These numbers highlight the model's accuracy, where the majority of predictions lie within a low error margin. Collectively, this comprehensive assessment establishes the high predictive capability and generalization power of the GEP model, making it a valuable and interpretable tool for estimating C-S in complex cementitious systems involving recycled and industrial by-products:

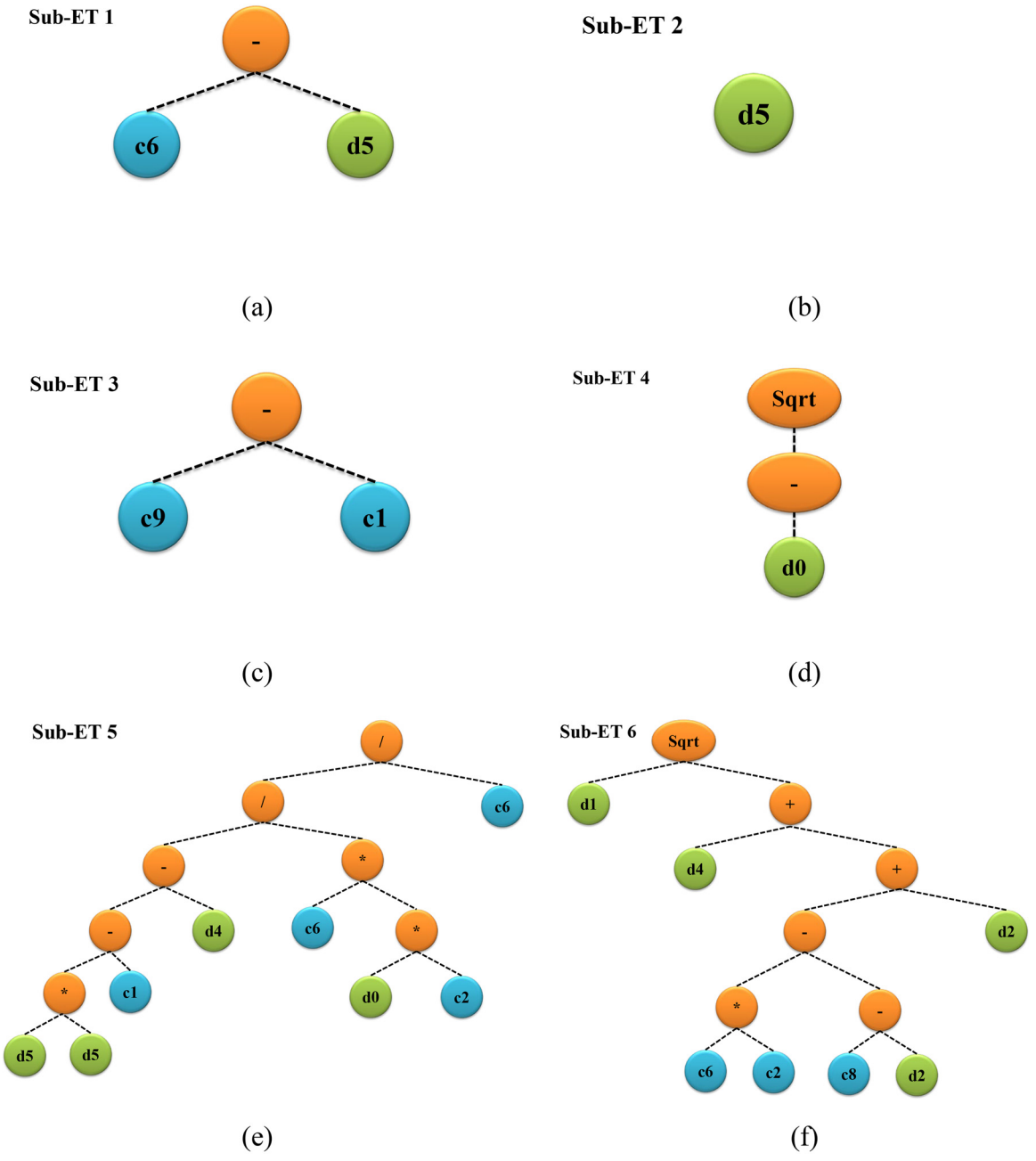

Figure 7: GEP model tree for C-S prediction: (a) Sub-ET 1, (b) Sub-ET 2, (c) Sub-ET 3, (d) Sub-ET 4, (e) Sub-ET 5, and (f) Sub-ET 6.

$$\text{C-S(MPa)} = 3.380 + \text{Gp} + \sqrt{\sqrt{\text{CM}}} + \left\{\frac{\text{Gp}^2 + 6.757 - \text{Mp}}{5.302^2 \cdot \text{CM} \cdot (-0.516)}\right\} + \sqrt{\text{Sd} - (\text{Mp} - 49.678 + 1.863 \cdot \text{Rb})}, \quad (8)$$

where CM represents cement, Sd represents sand, Rb represents rubber, S-F represents silica fume, Gp represents glass powder, Mp represents marble powder, and C-S represents compressive strength.

3.2 C-S MEP model

Eq. (9), generated using the MEP model, predicts the C-S of rubberized mortar based on six key inputs: CM, Sd, Rb, S-F, Gp, and Mp. Constructed using mathematical operators (+, −, ×, ÷, √, ^, e^x), the equation captures nonlinear relationships among the inputs. The first term reflects the interaction of SF with Sd and Rb, showing the pozzolanic contribution of SF in the presence of fine aggregates and recycled rubber. The nested square root term models the densification effect of

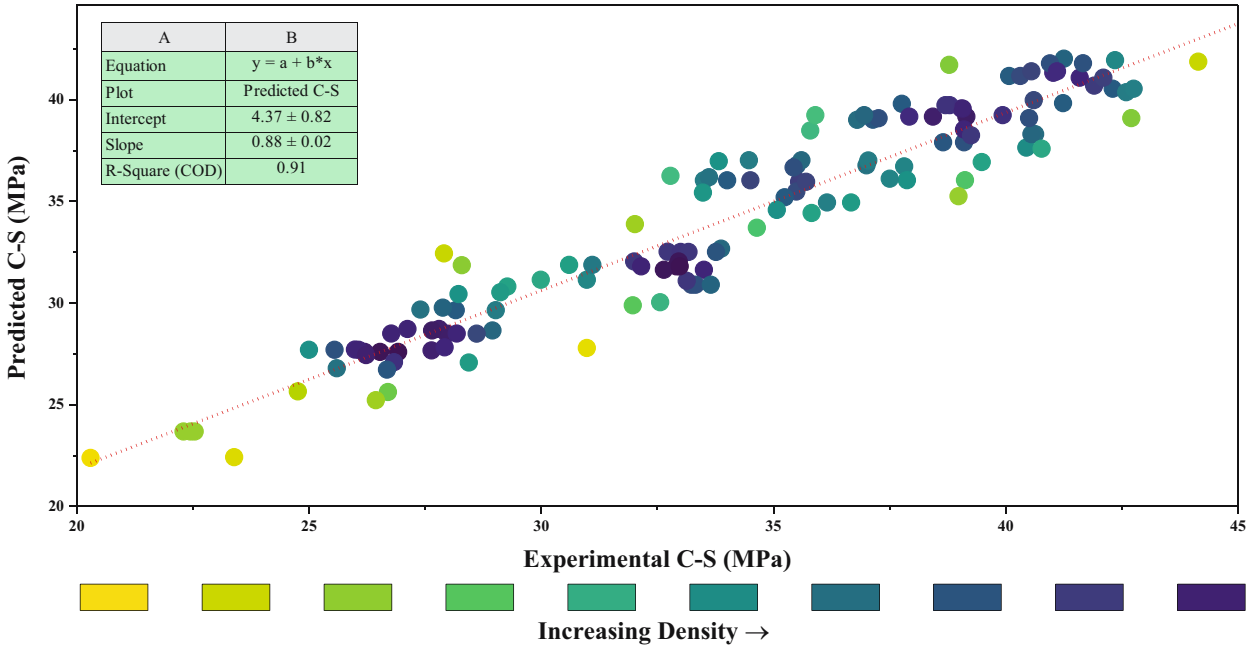

(a)

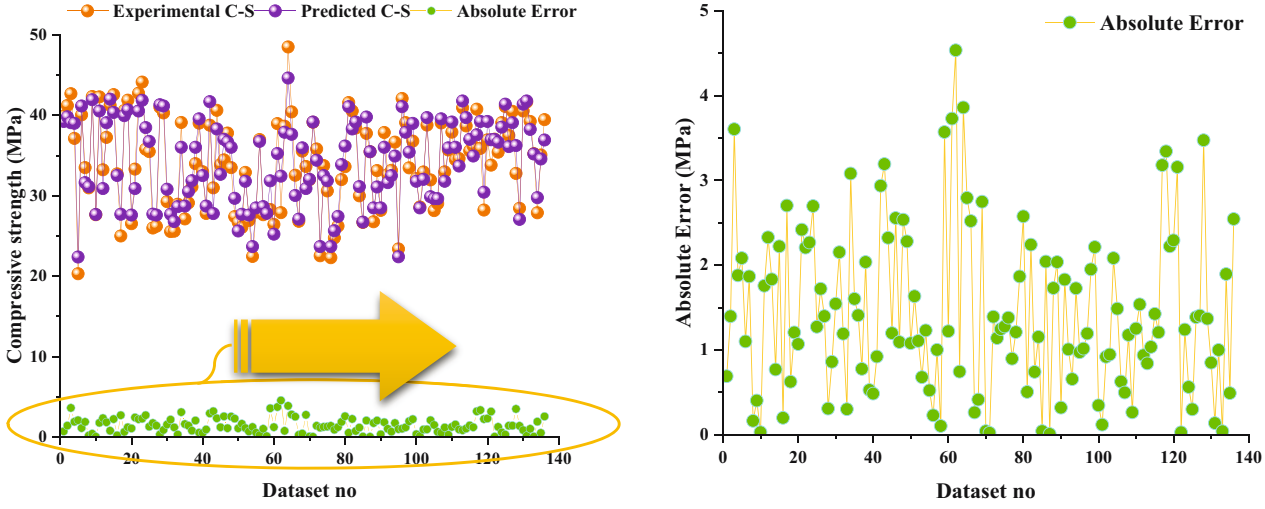

(b)

Figure 8: C-S GEP model: (a) correlation of predicted and observed C-S, and (b) predicted *vs* observed values and error distribution.

CM, Sd, and Rb. This equation offers a compact, interpretable, and accurate representation of how waste and supplementary materials influence the mortar strength:

$$\text{C-S(MPa)} = \left(\frac{\text{SF}}{\left(\frac{2 \cdot \text{Sd}}{\text{Sd} - 2 \cdot \text{CM} + \text{Rb}} + \text{SF} \right)} + \sqrt{\text{CM} + \text{Sd} - 3 \cdot \text{Rb}} \right) - \left(\frac{\left(\frac{2 \cdot \text{Sd}}{\text{Sd} - 2 \cdot \text{CM} + \text{Rb}} \right)}{\text{CM} - \text{Rb} - \text{Mp}} \right), \quad (9)$$

where CM represents cement, Sd represents sand, Rb represents rubber, S-F represents silica fume, Gp represents glass powder, Mp represents marble powder, and C-S represents compressive strength.

Figure 9(a) presents a scatter plot comparing the experimental and MEP-predicted C-S values, showing a strong correlation with a coefficient of determination R^2 of 0.95. The regression line closely follows the ideal 1:1 line, with a slope of 0.98 and an intercept of 0.63, indicating minimal deviation and high predictive accuracy. This performance surpasses that of the GEP model, which achieved a lower R^2 value of 0.91 under similar conditions. Figure 9(b) further supports the accuracy of the MEP model, showing a line plot of experimental and predicted values, along with the absolute error. The close overlap between estimated and test values across all data points and the

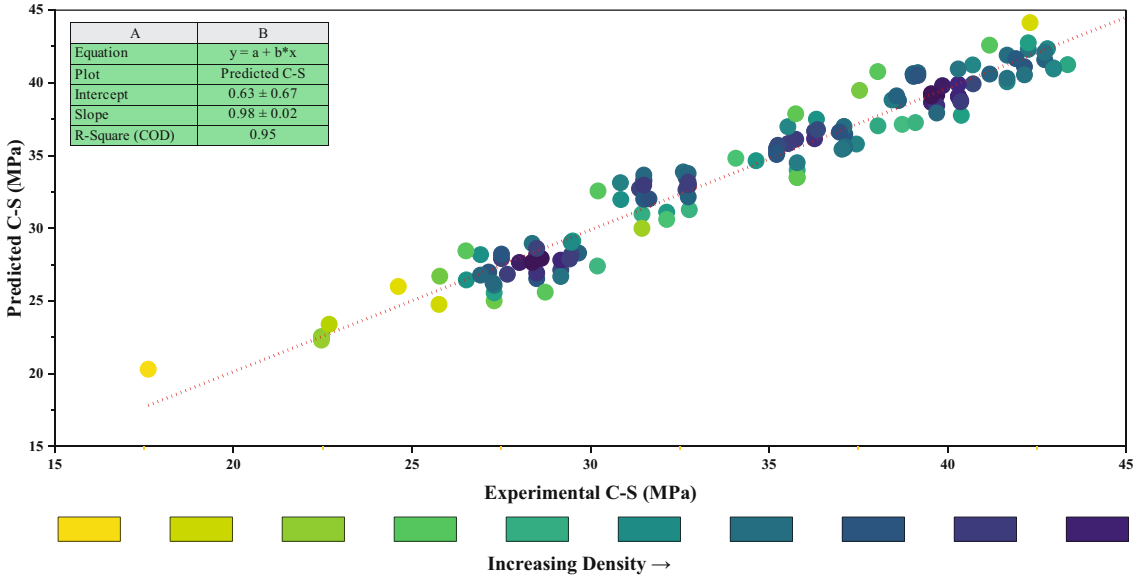

(a)

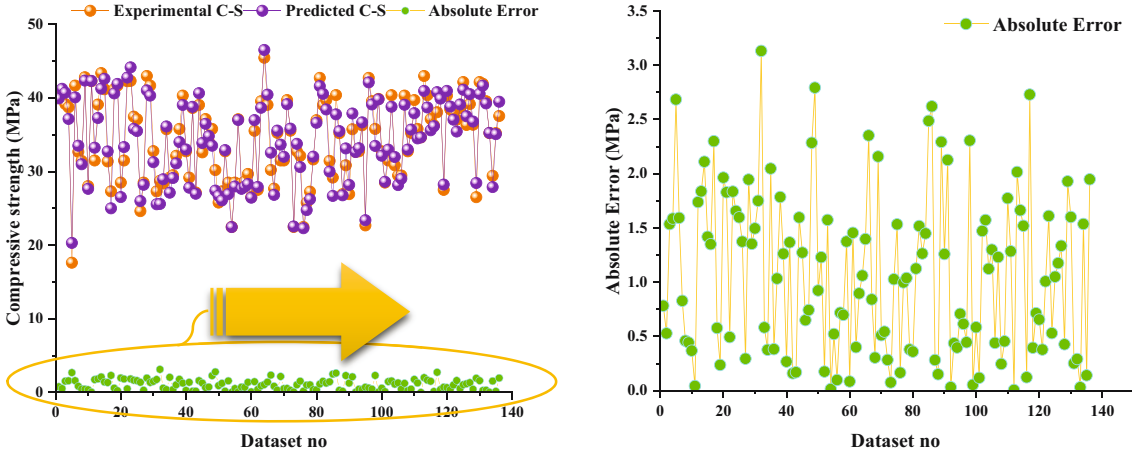

(b)

Figure 9: C-S MEP model: (a) correlation of predicted and observed C-S and (b) predicted *vs* observed values and error distribution.

relatively small and consistent absolute error demonstrate the model's robustness. The error distribution reveals that nearly 48% of the predictions have an error below 1 MPa, 40% fall within 1–2 MPa, and only 12% exceed 2 MPa, with an overall average error of just 1.069 MPa. These results collectively highlight the MEP model's superior predictive performance and generalization ability over the GEP model, confirming its reliability for estimating rubberized mortar compressive strength.

3.3 Statistical assessment of model accuracy

The results of the performance and error evaluations that were carried out utilizing the previously defined Eqs. (1)–(7) are displayed in Table 2. A variety of statistical indicators are used in these evaluations to thoroughly analyze the prediction capabilities of the models that were constructed. These indicators include RMSE, MAPE, NSE, *R*, MAE, PI, and OF. In every metric that was tested, the MEP model proved to be more effective than the GEP model. In comparison to GEP, which produced RMSE and MAE values of 2.066 and 1.666 MPa, respectively, the MEP model demonstrated superior numerical accuracy with values of 1.588 and 1.203 MPa, respectively. With a coefficient of determination (R) of 0.982 compared to 0.900 for the GEP model, the MEP model shows a far greater correlation between the experimental and projected values. The lower MAPE (3.026 *vs* 4.119%) of the MEP model further demonstrates its improved predictive dependability compared to the GEP model. The NSE value provided further evidence of this tendency; MEP achieved 0.961 compared to GEP's 0.796, indicating that MEP explained a larger amount of the observed data variance. The MEP model outperformed GEP in terms of optimization and generalizability, as evidenced by its higher PI value of 1.786 and lower OF value of 2.522 compared to 4.269, respectively. Figure 10 presents the Taylor's diagram, which visually summarizes the statistical performance of the developed models by comparing correlation, standard deviation, and centered RMSE. The MEP model exhibits a closer alignment with the reference point, indicating superior accuracy and predictive performance compared to the GEP model. This highlights MEP's enhanced capability in capturing the data trend more effectively. These findings collectively demonstrate that the MEP model offers a more accurate and robust framework for predicting the C-S of rubberized mortar, making it a promising tool for practical engineering applications and sustainable material design.

Table 2: Findings obtained by statistical analysis

Metric	Unit	C-S GEP	C-S MEP
RMSE	MPa	2.066	1.588
MAE	MPa	1.666	1.203
R	MPa	0.900	0.982
MAPE	%	4.119	3.026
NSE	MPa	0.796	0.961
PI	—	1.355	1.786
OF	—	4.269	2.522

3.4 PDPs

PDPs offer critical insights into how individual input variables influence the predicted C-S of rubberized mortar, while averaging out the effects of all other features. These plots are essential for understanding the model behavior and guiding mix design optimization. Figure 11(a) shows that increasing cement (CM) content generally enhances strength, aligning with its role as a primary binder. Figure 11(b) indicates that moderate sand (Sd) content supports strength gain, though excessive amounts may lead to a plateau or decline. Figure 11(c) reveals a negative impact of rubber (Rb) content on strength, reflecting the poor bonding characteristics of rubber particles. Figure 11(d) shows a nonlinear yet overall positive effect of silica fume (S-F), which improves the microstructure and strength up to an optimal dosage. Figure 11(e) demonstrates that marble powder (Mp) initially boosts strength, but further addition yields diminishing returns. Finally, Figure 11(f) highlights that glass powder (Gp) enhances strength moderately, contributing as a SCM, though its benefits saturate at higher dosages. Collectively, these 1D PDPs provide an

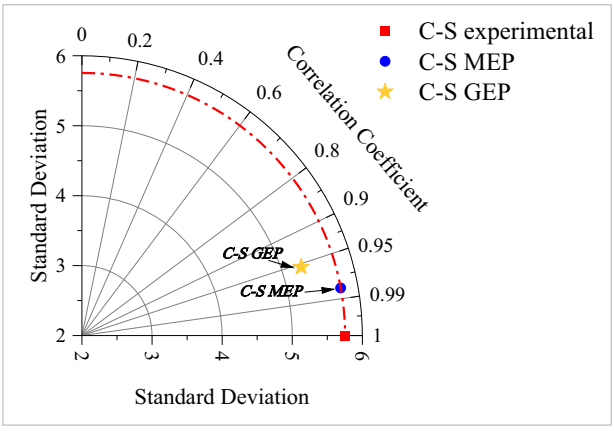

Figure 10: Taylor plot of model validation.

interpretable, data-driven foundation for optimizing mortar composition.

3.5 ICE

The ICE plots (Figure 12(a)–(f)) provide a detailed, instance-level view of how changes in each input feature influence the predicted C-S for individual samples. Unlike PDPs, which average the effects, ICE plots show a collection of curves, each representing a different data instance, allowing detection of heterogeneous behaviors and feature interactions. Figure 12(a) shows consistent upward trends in strength with increasing cement (CM), whereas Figure 12(b) reveals mixed responses to sand (Sd), suggesting that its role may vary depending on other mix components. Figure 12(c) confirms a generally declining strength with more rubber (Rb), though a few instances show resilience. Figure 12(d) illustrates that silica fume (S-F) boosts the strength in most cases, but some curves flatten, indicating a limit to its contribution. Figure 12(e) and (f) illustrates that the inclusion of glass powder (Gp) and marble powder (Mp), respectively, generally contributes to strength enhancement in the majority of cases. However, a few individual data patterns diverge from this trend, indicating the presence of complex and potentially non-linear interactions between these materials and other

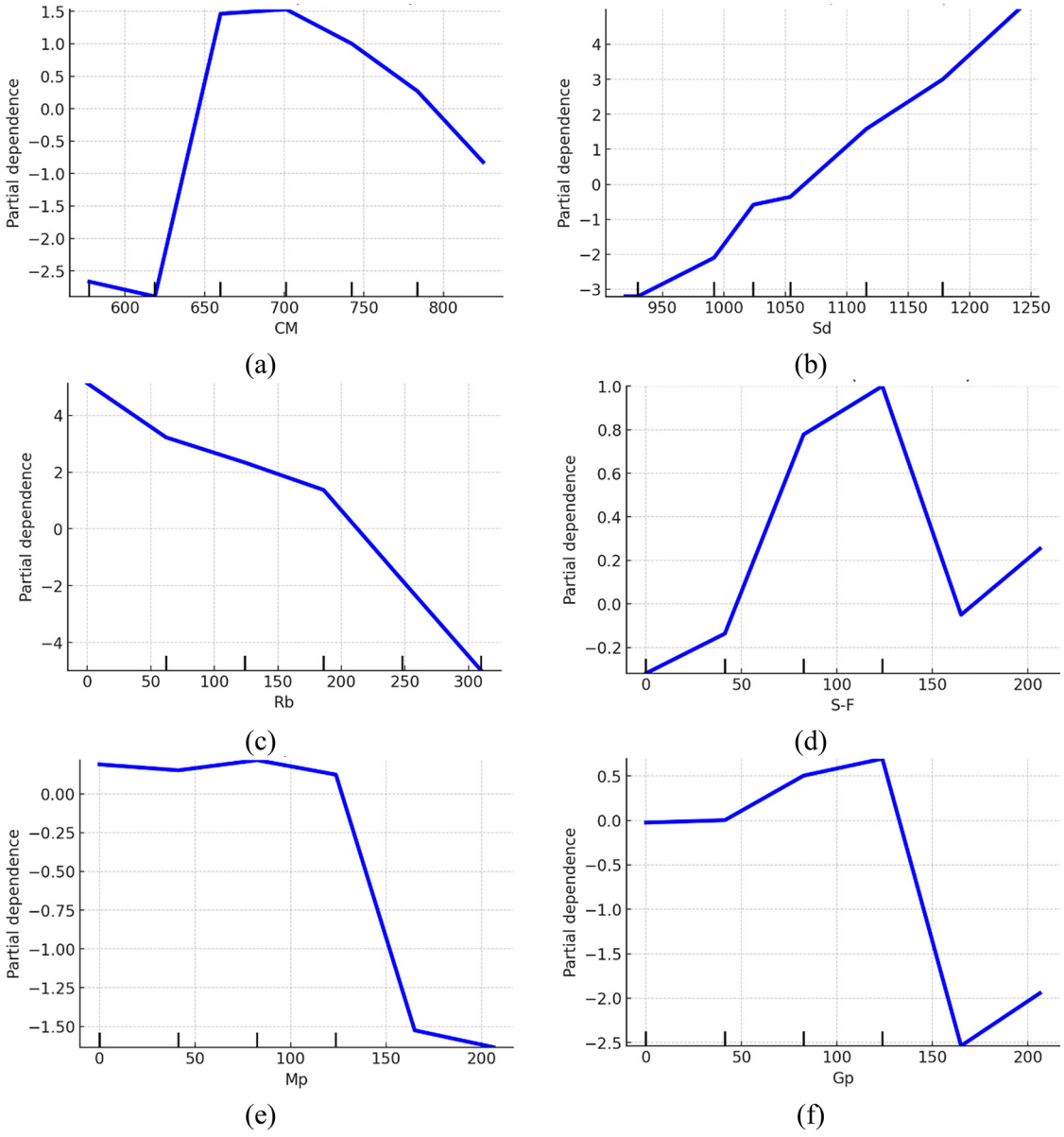

Figure 11: PDPs for rubberized mortar: (a) CM, (b) Sd, (c) Rb, (d) S-F, (e) Mp, and (f) Gp.

influencing variables. Overall, ICE plots complement PDPs by uncovering hidden variability and supporting more nuanced material design decisions.

4 Discussion

This study used two state-of-the-art ML methods, GEP and MEP, to forecast and optimize the C-S of rubberized mortar containing silica fume (S-F), marble powder (Mp), and glass powder (Gp). A robust dataset consisting of 408 data points, sourced from the existing literature and comprising six input variables and one output (compressive strength), was utilized to develop and train the models. The model's performance was validated using statistical metrics, Taylor's diagram, and R^2 values. The MEP model was clearly superior to the GEP model in terms of statistical performance, with a higher R value (0.982 *vs* 0.900), lower RMSE (1.588 *vs* 2.066 MPa), lower MAE (1.203 *vs* 1.666 MPa), and reduced MAPE (3.026 *vs* 4.119%). Additionally, the MEP model had a considerably higher NSE value (0.961 *vs* 0.796).

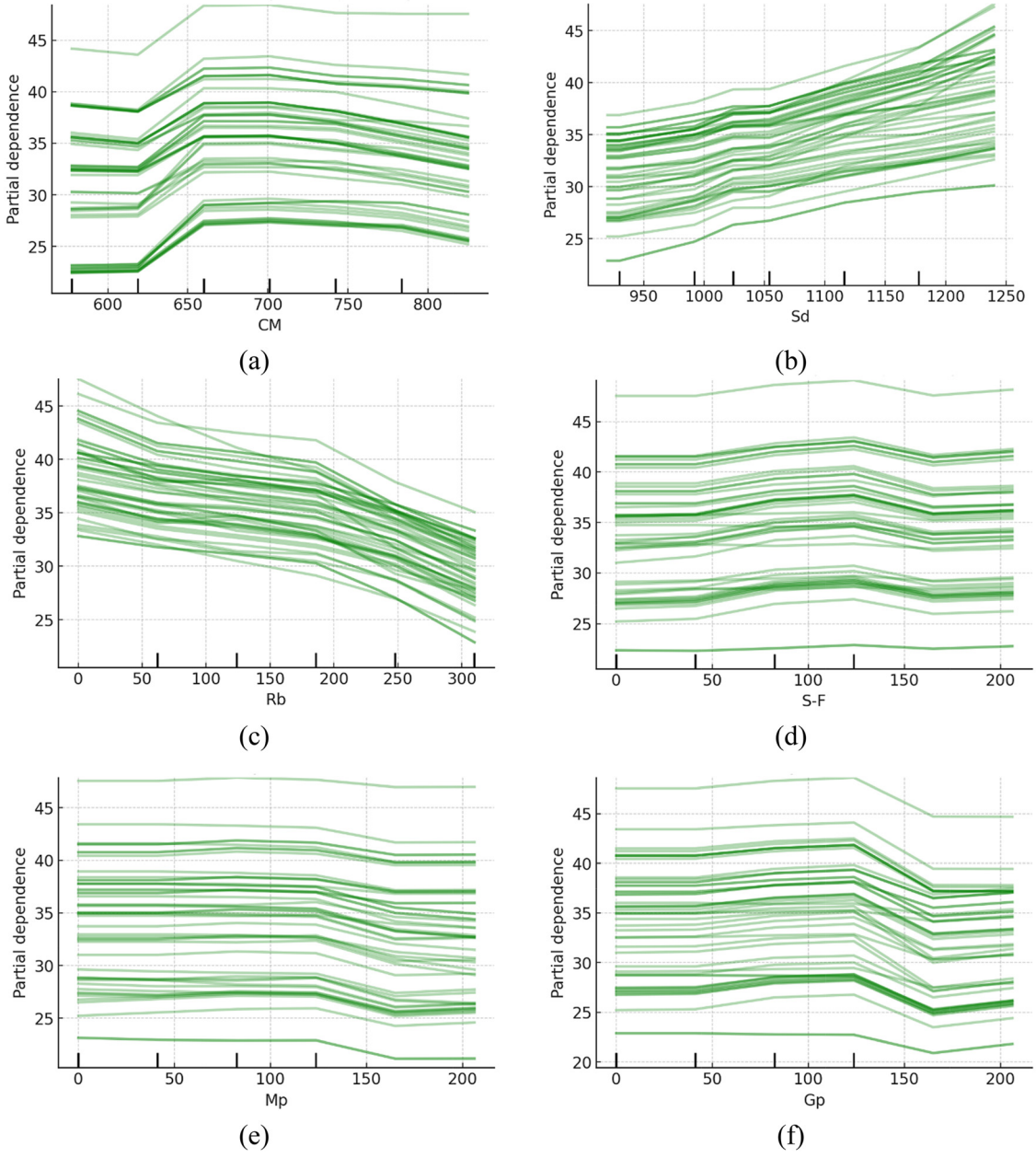

Figure 12: ICE plots for rubberized mortar: (a) CM, (b) Sd, (c) Rb, (d) S-F, (e) Mp, and (f) Gp.

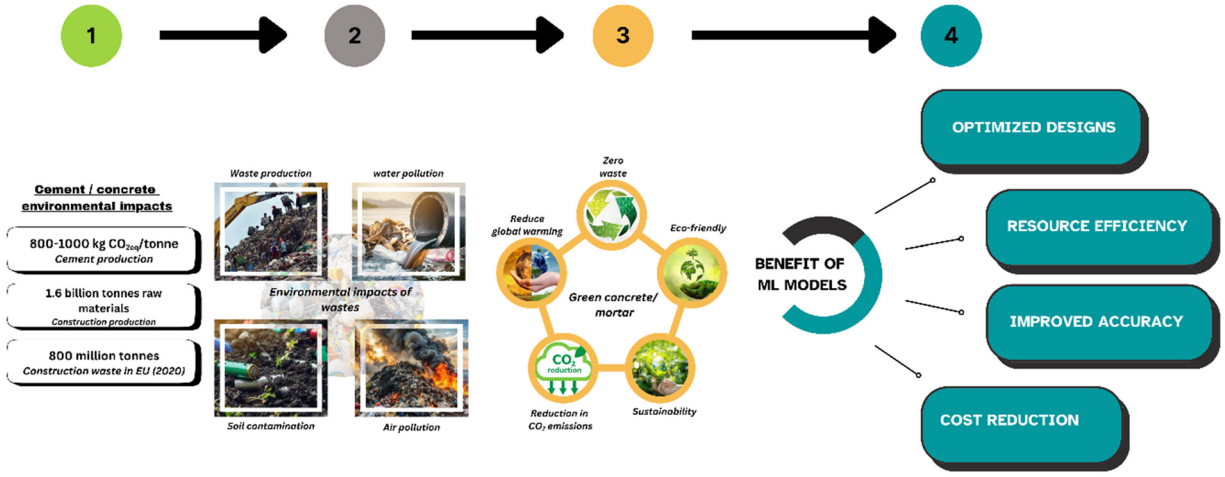

Figure 13: Framework illustrating green concrete development using waste materials and ML.

The MEP model was further validated as superior by the PI and OF, which had values of 1.786 and 2.522, respectively, compared to 1.355 and 4.269 for GEP. To enhance interpretability, PDPs were employed, which revealed clear trends such as the strength-enhancing role of cement and silica fume, and the detrimental impact of rubber content. Meanwhile, ICE plots complemented the PDPs by exposing instance-level variations and feature interactions, offering deeper insights into the mix behavior and model predictions. These findings are consistent with prior literature emphasizing the higher robustness and adaptability of MEP over traditional modeling techniques. In conclusion, the MEP model demonstrates a significant promise for application in complex material optimization studies, offering reliable, accurate, and interpretable predictions crucial for advancing sustainable construction practices. Figure 13 depicts the shift from traditional cement-based materials to sustainable green concrete/mortar using waste like rubber, glass, marble, and silica fume. This promotes a circular economy, reduces environmental impact, and leverages ML for optimized, efficient mix designs.

A distinctive strength of both MEP and GEP lies in their ability to handle complex, nonlinear datasets without oversimplifying relationships, making them particularly well-suited for modeling intricate behaviors in heterogeneous materials like rubberized mortar. Unlike many black-box ML models, these evolutionary algorithms not only deliver high prediction accuracy but also generate explicit mathematical expressions that describe the relationship between input features and output, offering transparency, interpretability, and practical applicability in engineering design. However, despite these advantages, there are notable limitations. First, consistency in input units is essential, as variations can significantly affect model performance. Second, the models can be sensitive to changes in the data set. Introducing new data or rebalancing existing points may alter developed equations and predictions. Third, these models still require domain expertise and manual oversight in setting parameters, interpreting results, and refining model structures. Additionally, overfitting can occur if model complexity is not properly regulated, and the derived equations, while interpretable, may become excessively large or nonlinear, reducing usability. As a way forward, future studies may benefit from incorporating more modern AI or hybrid ML techniques, such as ensemble learning or deep learning, to improve performance and generalization. Expanding the dataset by including more diverse mix designs or additional input variables, such as curing conditions, temperature effects, or water absorption, could further enhance the robustness of predictions. Moreover, investigating other critical properties of rubberized mortar, such as durability, workability, shrinkage, or thermal resistance, would provide a more holistic understanding of its performance and broaden the practical scope of these predictive models.

5 Conclusions

This study successfully applied GEP and MEP to predict the C-S of rubberized mortar incorporating silica fume, marble powder, and glass powder. The modeling process was supported by an extensive dataset and validated using various performance metrics and interpretability tools. The results not only demonstrated the superiority of the MEP model

but also offered deep insights into the influence of key input variables. Based on the findings, the following conclusions can be drawn:

- The MEP model demonstrated superior predictive accuracy for C-S with an R^2 value of 0.95, significantly outperforming the GEP model (R^2 = 0.91), confirming its reliability in modeling complex mortar systems.
- The MEP model was better at forecasting the C-S of rubberized mortar than the GEP model, according to performance criteria that compare the two models. It achieved higher accuracy (R = 0.982 *vs* 0.900), better efficiency (NSE = 0.961 *vs* 0.796), and lower errors (RMSE = 1.588 MPa *vs* 2.066 MPa; MAE = 1.203 MPa *vs* 1.666 MPa). Additionally, the MEP model demonstrated superior optimization capability with a higher PI and lower OF, confirming its robustness and suitability for sustainable material modeling.
- PDPs plots revealed that cement and silica fume positively influence C-S, while increasing rubber content shows a detrimental effect, offering interpretable insights into the role of each component.
- Complex feature interactions and the necessity for tailored mix designs are highlighted by ICE plot analysis, which shows that cement, silica fume, marble powder, and glass powder typically increase C-S, but their effects vary across instances, with diminishing or deviating trends in some cases. In contrast, rubber consistently reduces strength, and sand shows mixed influence.

The study's limitations include its reliance on a specific dataset, sensitivity to input unit consistency, and focus solely on C-S. Future work should expand datasets, investigate other mechanical and durability properties, and explore modern or hybrid AI techniques to improve model generalizability and practical applicability.

Acknowledgments: The authors acknowledge the Science and Technology Tackling Project of Henan Province (Project no: 242102210123) and the Science and Technology Tackling Project of Henan Province (Project no: 242102321090). The authors extend their appreciation to Taif University, Saudi Arabia, for supporting this work through project number TU-DSPP-2024-248.

Funding information: This research was funded by Science and Technology Tackling Project of Henan Province (Project no: 242102210123), Science and Technology Tackling Project of Henan Province (Project no: 242102321090), and the authors extend their appreciation to Taif University, Saudi Arabia, for supporting this work through project number TU-DSPP-2024-248.

Author contributions: Y.Z.: conceptualization, formal analysis, supervision, validation, and writing – original draft. Q.Z.: data acquisition, resources, methodology, visualization, writing, reviewing, and editing. M.A.: project administration, formal analysis, software, resources, writing, reviewing, and editing. A.H.A.: software, validation, data acquisition, conceptualization, writing, reviewing, and editing. A.A.A.E.: methodology, supervision, visualization, formal analysis, writing, reviewing, and editing. All authors have accepted responsibility for the entire content of this manuscript and approved its submission.

Conflict of interest: The authors state no conflict of interest.

Data availability statement: The dataset generated and/or analyzed during the current study is available from the corresponding author upon reasonable request.

References

[1] Peng, C. Calculation of a building's life cycle carbon emissions based on Ecotect and building information modeling. *Journal of Cleaner Production*, Vol. 112, 2016, pp. 453–465.

[2] Asif, U., M. F. Javed, D. M. Alsekait, D. S. AbdElminaam, and H. Alabduljabbar. Toward sustainability: Integrating experimental study and data-driven modeling for eco-friendly paver blocks containing plastic waste. *Reviews on Advanced Materials Science*, Vol. 63, 2024, id. 20240051.

[3] Ahmad, W., S. J. McCormack, and A. Byrne. Biocomposites for sustainable construction: A review of material properties, applications, research gaps, and contribution to circular economy. *Journal of Building Engineering*, Vol. 105, 2025, id. 112525.

[4] Wu, Y.-F., S. M. S. Kazmi, M. J. Munir, Y. Zhou, and F. Xing. Effect of compression casting method on the compressive strength, elastic modulus and microstructure of rubber concrete. *Journal of Cleaner Production*, Vol. 264, 2020, id. 121746.

[5] Ozkilic, Y. O., O. Zeybek, M. Karalar, A. I. Celik, and E. Althaqafi. Experimental and ARX model-based prediction of concrete strength with waste marble powder as replacement of aggregates. *Structural Engineering and Mechanics*, Vol. 95, 2025, pp. 15–30.

[6] Bouchelil, L., S. B. S. Jafar, and M. Khanzadeh Moradllo. Evaluating the performance of internally cured limestone calcined clay concrete mixtures. *Journal of Sustainable Cement-Based Materials*, Vol. 14, 2025, pp. 198–208.

[7] Tang, B., H. Wu, and Y.-F. Wu. Evaluation of carbon footprint of compression cast waste rubber concrete based on LCA approach. *Journal of Building Engineering*, Vol. 86, 2024, id. 108818.

[8] Başaran, B., C. Aksoylu, Y. O. Özkılıç, M. Karalar, and A. Hakamy. Shear behaviour of reinforced concrete beams utilizing waste marble powder, *Structures*, Vol. 54, 2023, pp. 1090–1100.

[9] Wang, Q.-Z., N.-N. Wang, M.-L. Tseng, Y.-M. Huang, and N.-L. Li. Waste tire recycling assessment: Road application potential and

carbon emissions reduction analysis of crumb rubber modified asphalt in China. *Journal of Cleaner Production*, Vol. 249, 2020, id. 119411.
[10] Karalar, M., B. Başaran, C. Aksoylu, Ö. Zeybek, E. Althaqafi, A. N. Beskopylny, et al. Utilizing recycled glass powder in reinforced concrete beams: comparison of shear performance. *Scientific Reports*, Vol. 15, 2025, id. 6919.
[11] Murali, G., L. Poka, K. Parthiban, M. K. Haridharan, and A. Siva. Impact response of novel fibre-reinforced grouted aggregate rubberized concrete. *Arabian Journal for Science and Engineering*, Vol. 44, 2019, pp. 8451–8463.
[12] Shahjalal, M., K. Islam, T. Ahmed, and R. Ahsan. Mechanical characterization of fiber-reinforced rubberized recycled concrete. *Construction and Building Materials*, Vol. 412, 2024, id. 134799.
[13] Su, J.-Y., G. Chen, H.-S. Pan, J.-X. Lin, J. Zhang, K.-X. Zhuo, et al. Rubber modified high strength-high ductility concrete: Effect of rubber replacement ratio and fiber length. *Construction and Building Materials*, Vol. 404, 2023, id. 133243.
[14] Cr, S. B. and P. Kathirvel. Development of ternary blended rubberized cement mortar. *Materials Today: Proceedings*, Vol. 43, 2021, pp. 1241–1245.
[15] Karimi, H. R., M. R. M. Aliha, E. Khedri, A. Mousavi, S. M. Salehi, P. J. Haghighatpour, et al. Strength and cracking resistance of concrete containing different percentages and sizes of recycled tire rubber granules. *Journal of Building Engineering*, Vol. 67, 2023, id. 106033.
[16] Mei, J., G. Xu, W. Ahmad, K. Khan, M. N. Amin, F. Aslam, et al. Promoting sustainable materials using recycled rubber in concrete: A review. *Journal of Cleaner Production*, Vol. 373, 2022, id. 133927.
[17] Moasas, A. M., M. N. Amin, K. Khan, W. Ahmad, M. N. A. Al-Hashem, A. F. Deifalla, et al. A worldwide development in the accumulation of waste tires and its utilization in concrete as a sustainable construction material: A review. *Case Studies in Construction Materials*, Vol. 17, 2022, id. e01677.
[18] Karalar, M., H. Öztürk, and Y. O. Özkılıç. Experimental and numerical investigation on flexural response of reinforced rubberized concrete beams using waste tire rubber. *Steel and Composite Structures*, 2022, pp. 43–57.
[19] Khan, K., W. Ahmad, M. N. Amin, A. Ahmad, S. Nazar, A. A. Alabdullah, et al. Exploring the use of waste marble powder in concrete and predicting its strength with different advanced algorithms. *Materials*, Vol. 15, 2022, id. 4108.
[20] Chatbi, M., Z. R. Harrat, M. A. Benatta, B. Krour, M. Hadzima-Nyarko, E. Işık, et al. Nano-clay platelet integration for enhanced bending performance of concrete beams resting on elastic foundation: an analytical investigation. *Materials*, Vol. 16, 2023, id. 5040.
[21] Zhao, S. and Q. Zhang. Effect of silica fume in concrete on mechanical properties and dynamic behaviors under impact loading. *Materials*, Vol. 12, 2019, id. 3263.
[22] Murali, G., A. K. Nassar, M. Swaminathan, P. Kathirvel, and L. S. Wong. Effect of silica fume and glass powder for enhanced impact resistance in GGBFS-based ultra high-performance geopolymer fibrous concrete: An experimental and statistical analysis. *Defence Technology*, Vol. 41, 2024, pp. 59–81.
[23] Waqar, A., M. B. Khan, M. T. Afzal, D. Radu, T. Gălăţanu, C. E. Cazacu, et al. Investigating the synergistic effects of carbon fiber and silica fume on concrete strength and eco-efficiency. *Case Studies in Construction Materials*, Vol. 20, 2024, id. e02967.
[24] Lou, Y., K. Khan, M. N. Amin, W. Ahmad, A. F. Deifalla, and A. Ahmad. Performance characteristics of cementitious composites modified with silica fume: A systematic review. *Case Studies in Construction Materials*, Vol. 18, 2023, id. e01753.
[25] Yildizel, S. A., Y. O. Özkılıç, and A. Yavuz. Optimization of waste tyre steel fiber and rubber added foam concretes using Taguchi method and artificial neural networks, *Structures*, Vol. 61, 2024, id. 106098.
[26] Marani, A., A. Jamali, and M. L. Nehdi. Predicting ultra-high-performance concrete compressive strength using tabular generative adversarial networks. *Materials*, Vol. 13, 2020, id. 4757.
[27] Marani, A. and M. L. Nehdi. Machine learning prediction of compressive strength for phase change materials integrated cementitious composites. *Construction and Building Materials*, Vol. 265, 2020, id. 120286.
[28] Nunez, I., A. Marani, and M. L. Nehdi. Mixture optimization of recycled aggregate concrete using a hybrid machine learning model. *Materials*, Vol. 13, 2020, id. 4331.
[29] Zhang, J., Y. Huang, F. Aslani, G. Ma, and B. Nener. A hybrid intelligent system for designing optimal proportions of recycled aggregate concrete. *Journal of Cleaner Production*, Vol. 273, 2020, id. 122922.
[30] Zhang, J., D. Li, and Y. Wang. Toward intelligent construction: Prediction of mechanical properties of manufactured-sand concrete using tree-based models. *Journal of Cleaner Production*, Vol. 258, 2020, id. 120665.
[31] Rajasekar, A., K. Arunachalam, and M. Kottaisamy. Assessment of strength and durability characteristics of copper slag incorporated ultra high strength concrete. *Journal of Cleaner Production*, Vol. 208, 2019, pp. 402–414.
[32] Naseri, H., H. Jahanbakhsh, P. Hosseini, and F. M. Nejad. Designing a sustainable concrete mixture by developing a new machine learning technique. *Journal of Cleaner Production*, Vol. 258, 2020, id. 120578.
[33] Young, B. A., A. Hall, L. Pilon, P. Gupta, and G. Sant. Can the compressive strength of concrete be estimated from knowledge of the mixture proportions?: New insights from statistical analysis and machine learning methods. *Cement and Concrete Research*, Vol. 115, 2019, pp. 379–388.
[34] Ahmad, W., V. S. S. C. S. Veeraghantla, and A. Byrne. Advancing sustainable concrete using biochar: Experimental and modelling study for mechanical strength evaluation. *Sustainability*, Vol. 17, 2025, id. 2516.
[35] Inqiad, W. B., M. S. Siddique, S. S. Alarifi, M. J. Butt, T. Najeh, and Y. J. H. Gamil. Comparative analysis of various machine learning algorithms to predict 28-day compressive strength of Self-compacting concrete. *Heliyon*, Vol. 9, 2023, id. e22036.
[36] Amin, M. N., R.-U.-D. Nassar, K. Khan, S. Ul Arifeen, M. Khan, and M. T. Qadir. Integrating testing and modeling methods to examine the feasibility of blended waste materials for the compressive strength of rubberized mortar. *Reviews on Advanced Materials Science*, Vol. 63, 2024, id. 20240081.
[37] Amin, M. N., A. A. A. Al-Naghi, R.-U.-D. Nassar, O. Algassem, S. A. Khan, and A. F. Deifalla. Investigating the rheological characteristics of alkali-activated concrete using contemporary artificial intelligence approaches. *Reviews on Advanced Materials Science*, Vol. 63, 2024, id. 20240006.
[38] Ilyas, I., A. Zafar, M. Afzal, M. Javed, R. Alrowais, F. Althoey, et al. Advanced machine learning modeling approach for prediction of compressive strength of FRP confined concrete using multiphysics genetic expression programming. *Polymers*, Vol. 14, 2022, id. 1789.
[39] Iftikhar, B., S. C. Alih, M. Vafaei, M. A. Elkotb, M. Shutaywi, M. F. Javed, et al. Predictive modeling of compressive strength of

sustainable rice husk ash concrete: Ensemble learner optimization and comparison. *Journal of Cleaner Production*, Vol. 348, 2022, id. 131285.

[40] Sarveghadi, M., A. H. Gandomi, H. Bolandi, and A. H. Alavi. Development of prediction models for shear strength of SFRCB using a machine learning approach. *Neural Computing and Applications*, Vol. 31, 2019, pp. 2085–2094.

[41] Lee, B. C. and D. M. Brooks. Accurate and efficient regression modeling for microarchitectural performance and power prediction. *ACM SIGOPS Operating Systems Review*, Vol. 40, 2006, pp. 185–194.

[42] Khawaja, L., M. F. Javed, U. Asif, L. Alkhattabi, B. Ahmed, and H. Alabduljabbar. Indirect estimation of resilient modulus (Mr) of subgrade soil: Gene expression programming vs multi expression programming, *Structures*, Vol. 66, 2024, id. 106837.

[43] Nematzadeh, M., A. A. Shahmansouri, and M. Fakoor. Post-fire compressive strength of recycled PET aggregate concrete reinforced with steel fibers: Optimization and prediction via RSM and GEP. *Construction and Building Materials*, Vol. 252, 2020, id. 119057.

[44] Amin, M. N., W. Ahmad, K. Khan, and A. F. Deifalla. Optimizing compressive strength prediction models for rice husk ash concrete with evolutionary machine intelligence techniques. *Case Studies in Construction Materials*, Vol. 18, 2023, id. e02102.

[45] Guan, Q. T., Z. L. Tong, M. N. Amin, B. Iftikhar, M. T. Qadir, and K. Khan. Analyzing the efficacy of waste marble and glass powder for the compressive strength of self-compacting concrete using machine learning strategies. *Reviews on Advanced Materials Science*, Vol. 63, 2024, id. 20240043.

[46] Iqbal, M. F., Q.-F. Liu, I. Azim, X. Zhu, J. Yang, M. F. Javed, et al. Prediction of mechanical properties of green concrete incorporating waste foundry sand based on gene expression programming. *Journal of Hazardous Materials*, Vol. 384, 2020, id. 121322.

[47] Mohammadzadeh S, D., S.-F. Kazemi, A. Mosavi, E. Nasseralshariati, and J. H. M. Tah. Prediction of compression index of fine-grained soils using a gene expression programming model. *Infrastructures*, Vol. 4, 2019, id. 26.

[48] Shahin, M. A. *Genetic programming for modelling of geotechnical engineering systems*, Springer, Switzerland, 2015.

[49] Çanakcı, H., A. Baykasoğlu, and H. Güllü. Prediction of compressive and tensile strength of Gaziantep basalts via neural networks and gene expression programming. *Neural Computing and Applications*, Vol. 18, 2009, pp. 1031–1041.

[50] Alade, I. O., M. A. Abd Rahman, and T. A. Saleh. Predicting the specific heat capacity of alumina/ethylene glycol nanofluids using support vector regression model optimized with Bayesian algorithm. *Solar Energy*, Vol. 183, 2019, pp. 74–82.

[51] Alade, I. O., A. Bagudu, T. A. Oyehan, M. A. Abd Rahman, T. A. Saleh, and S. O. Olatunji. Estimating the refractive index of oxygenated and deoxygenated hemoglobin using genetic algorithm–support vector regression model. *Computer Methods and Programs in Biomedicine*, Vol. 163, 2018, pp. 135–142.

[52] Zhang, W., R. Zhang, C. Wu, A. T. C. Goh, S. Lacasse, Z. Liu, et al. State-of-the-art review of soft computing applications in underground excavations. *Geoscience Frontiers*, Vol. 11, 2020, pp. 1095–1106.

[53] Alavi, A. H., A. H. Gandomi, H. C. Nejad, A. Mollahasani, and A. Rashed. Design equations for prediction of pressuremeter soil deformation moduli utilizing expression programming systems. *Neural Computing and Applications*, Vol. 23, 2013, pp. 1771–1786.

[54] Kisi, O., J. Shiri, and M. Tombul. Modeling rainfall-runoff process using soft computing techniques. *Computers & Geosciences*, Vol. 51, 2013, pp. 108–117.

[55] Alade, I. O., M. A. Abd Rahman, and T. A. Saleh. Modeling and prediction of the specific heat capacity of Al_2O_3/water nanofluids using hybrid genetic algorithm/support vector regression model. *Nano-Structures & Nano-Objects*, Vol. 17, 2019, pp. 103–111.

[56] Shahin, M. A. Use of evolutionary computing for modelling some complex problems in geotechnical engineering. *Geomechanics and Geoengineering*, Vol. 10, 2015, pp. 109–125.

[57] Gandomi, A. H. and D. A. Roke. Assessment of artificial neural network and genetic programming as predictive tools. *Advances in Engineering Software*, Vol. 88, 2015, pp. 63–72.

[58] Band, S. S., E. Heggy, S. M. Bateni, H. Karami, M. Rabiee, S. Samadianfard, et al. Groundwater level prediction in arid areas using wavelet analysis and Gaussian process regression. *Engineering Applications of Computational Fluid Mechanics*, Vol. 15, 2021, pp. 1147–1158.

[59] Taylor, K. E. Summarizing multiple aspects of model performance in a single diagram. *Journal of Geophysical Research: Atmospheres*, Vol. 106, 2001, pp. 7183–7192.